Observation of the whole Thomson scattering spectrum of laser-produced plasmas for EUV light sources

Yuta SATO[*1,†] Raimu FUKADA[*1] Fumitaka ITO[*1]
Kentaero TOMITA[*2] and Kiichiro UCHINO[*2]
†E-mail of corresponding author:3ES16011G@s.kyushu-u.ac.jp

The whole spectrum including the ion feature and the electron feature of collective Thomson scattering from laser-produced tin plasmas for EUV light sources has been observed for the first time. The purpose is to realize the evaluation of electron density, electron temperature, ion temperature and average ionic charge of the plasmas at the same time. Since the intensity of the electron feature is very weak compared with self-emissions from the plasma, efforts were concentrated to detect the peak wavelength of the electron feature. By applying the spectrometer system appropriately designed and optimizing the scattering geometry, it was achieved to detect the peak of the electron feature with the signal-to-noise ratio larger than one.

Key words: *EUV lithography, laser Thomson scattering*

1. Introduction

Extreme ultraviolet (EUV) lithography is a promising technology for high-volume manufacturing of next-generation semiconductor devices.[1-4] Laser-produced tin (Sn) plasma is being considered as a strong candidate of EUV light sources. A carbon dioxide (CO_2) drive laser and a Sn droplet target are employed as an efficient EUV light source. In order to put it into practical use, the primary challenge involves the improvement of the conversion efficiency (CE) of EUV light sources with respect to the output of CO_2 lasers. Plasma parameters, such as electron density (n_e), electron temperature (T_e), and average ionic charge (Z) [5,6] are important because the EUV emissivity strongly depends on them. In order to measure these parameters, a collective laser Thomson scattering (LTS) system, which is tuned to detect the ion feature spectra, has been developed.[7,8] This system revealed time-resolved two-dimensional profiles of n_e, T_i, and Z of Sn plasmas.[9,10] Here, we assumed $T_i = T_e$. The ion feature is not enough to fix the four parameters, because the ion feature has only three information,

i.e., absolute signal intensity, a width between two peaks and a dip between them. In order to evaluate the four parameters without any assumption, simultaneous detections of the ion feature and the electron feature are required. Therefore, we tried to detect both the ion feature and the electron feature of the Thomson scattering spectrum from the plasma which has the parameters of the EUV light source plasma.

To detect both features, there are two things which should be considered. One is differences in spectral widths of the two features. An estimated spectral width of the ion feature from the typical EUV light source plasma (n_e, T_e, T_i, and Z are 10^{24} m^{-3}, 30 eV, 30 eV, and 10, respectively) is 200 pm. On the other hand, the width of the electron feature is estimated to be 10 nm. To realize simultaneous measurements, we decided to fabricate two different spectrometers which are suitable for the ion feature and the electron feature. The other problem is a very small intensity of the electron feature compared to the noise level of the bremsstrahlung radiation from the plasma.[11-13] Because the peak wavelength of the electron feature of collective Thomson scattering gives information about the electron density and the electron temperature, we concentrated to detect the

*1   Department of Applied Science for Electronics and Materials, Graduate Student
*2   Department of Electrical and Material Science

peak wavelength of the electron feature in this study. By optimizing the scattering geometry, we finally succeeded to detect the peak of the electron feature with the signal-to-noise ratio larger than one.

2.　Collective Thomson scattering

The theory of Thomson scattering has been extensively described in Ref. 14. Here we only describe the principle to the extent necessary to understand the situation of LTS for this study. When a visible laser is used as a probing laser, the predicted LTS spectra from laser produced Sn plasmas lie in the collective regime, in which the scattering parameter a is larger than 1 [$a = (k\lambda_D)^{-1}$, where λ_D is the Debye length and k is the wavenumber of the scattered light]. In the collective regime, a LTS spectrum consists of an ion feature and an electron feature.

For the case of ion feature, the shape reflects the ion-acoustic-wave frequency $\omega_{ac} = k\sqrt{(a^2/1 + a^2)(Z\kappa T_e + 3\kappa T_i/m_i)}$, where κ is the Boltzmann constant, m_i is the ion mass. The spectrum also exhibits two peaks with a dip between them. The width between the two peaks is related to the probing laser wavelength λ_0, the speed of light c, and ω_{ac}, and is expressed as $2\Delta\lambda_{\text{peak-i}}$ $\left[\Delta\lambda_{\text{peak-i}} = (\lambda_0^2/2\pi c)\omega_{ac}\right]$. By determining $\Delta\lambda_{\text{peak-i}}$ and the spectral shape, which is characterized by ion-acoustic wave damping, a product of Z and T_e (ZT_e), and T_i can be obtained. In addition, it is possible to estimate n_e as a zeroth order value by performing the absolute calibration of signal intensity, because the intensity of the ion feature is strongly related to n_e and is proportional a dynamic form factors $S_i = Za^4/[(1 + a^2)\{1 + a^2(1 + ZT_e/T_i)\}]$. For the case of the electron feature, the spectrum is also characterized by two peaks, and the angular frequency at which the peak appears is expressed as $\Delta\omega = \sqrt{n_e e^2/m_e\varepsilon_0 + 3\kappa T_e k^2/m_e}$, where ε_0 is the dielectric constant of vacuum. The wavelength difference ($\Delta\lambda_{\text{peak-e}}$) from λ_0 is expressed as $\Delta\lambda_{\text{peak-e}} = (\lambda_0^2/2\pi c)\Delta\omega$. The intensity of the electron feature is also strongly related to n_e and is proportional a dynamic form factors $S_e = 1/(1 + a^2)$.

3.　Experimental setup

Figure 1 shows a schematic diagram of the experimental setup. The x, y, and z axes are defined in Fig. 1. Two different lasers were used to generate plasma. A first laser was a Nd:YAG laser (Continuum Surelite II, pulse width: 10 ns full width at half maximum (FWHM), laser energy: 320 mJ, wavelength: 1064 nm, typical spot diameter: 200 μm) and propagated in the z axis. Sn plasma was produced by the first laser. A second laser was also a Nd:YAG laser (Continuum Surelite II, pulse width: 10 ns full width at half maximum (FWHM), laser energy: 320 mJ, wavelength: 1064 nm, typical spot diameter: 80 μm), which was used to heat the plasmas. In this paper, we refer to the first and the second lasers as the driving laser and heating laser, respectively. After the Sn plasma was heated by the heating laser, a probing laser was injected into the plasma for LTS measurements. The probing laser was a second-harmonic Nd:YAG laser with injection seeding (Continuum Powerlite 9010 with an injection seeder; spectral spread <0.1 pm, pulse width: 8 ns FWHM, laser energy: 10 mJ, wavelength $\lambda_0 = 532$ nm, typical spot diameter: 50 μm). The time zero (t = 0 ns) for the LTS measurements was the peak of the driving laser. The heating and the probing lasers were injected at $t = 97$ ns and $t = 100$ ns, respectively. The two lasers were injected co-axially along the x axis and were focused at the same position above the target surface by an achromatic lens with the same focal length ($f = 150$ mm). A tin plate target was set in the vacuum chamber (<10^{-2} Torr) at z = -150 μm and a thin edge face (thickness 100 μm) was used as the
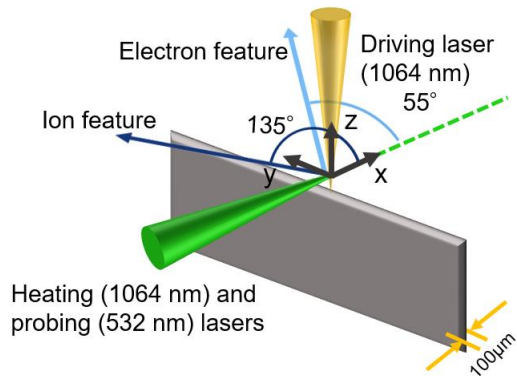

Fig. 1　Schematic diagram of experimental setup

laser-irradiated surface. This thickness was selected so as to reduce the amount of the plasma self-emission.

The ion feature and the electron feature were collected by two different achromatic lenses at angles of 135° and 55° with respect to the incidence angle of the probing laser, respectively, as shown in Fig.1. Then, the LTS signals were focused on the entrance slit of the two spectrometers for the ion feature and the electron feature. The spectrometer for the ion feature was same as that described in Ref. 9. The spectrometer having 6 gratings achieved a 12 pm spectral resolution and a sufficient stray-light rejection (10^{-4}) with a very narrow wavelength block range [within ±14 pm from λ_0 (= 532 nm)]. The gate width of a detector, which was an intensified charge-coupled device (ICCD) camera (quantum efficiency: 35% at 532 nm), was set to 3 ns. A conventional triple-grating spectrometer (TGS) was utilized for electron feature measurements. The TGS mainly consisted of six achromatic lenses (L1: f = 250 mm, L2-L5: f = 170 mm, L6: f = 220 mm effective diameter: 46 mm), three diffraction gratings (1200 grooves/mm, effective area: 56 mm × 56 mm), an entrance slit (width: 60 μm), an intermediate slit (width: 200 μm), and a thin tungsten wire (diameter: 500 μm) to block the stray light. Another ICCD camera (quantum efficiency: 45 % at 532 nm, gate width: 2ns) was used as a detector. With the TGS, a spectral resolution of 0.37 nm and a sufficient stray-light rejection at ±1.5 nm from λ_0 were achieved. We note that the absolute calibration of both the ion feature and electron feature was performed by Rayleigh scattering measurements from nitrogen gas.

4.　Results

Figure 2(a) shows the ion feature image detected by the ICCD camera. Figure 2(b) shows the LTS spectrum extracted from the Fig. 2(a). The spectrum was successfully fitted by a theoretical curve, as shown in Fig. 2(b). From the fitting curve and the absolute calibration, n_e, ZT_e, and T_i were fixed to be 1.0×10^{24} m^{-3}, 271, and 25 eV, respectively.

At the final stage of the spectrometer for

the electron feature was divided into 2 optical paths using a polarization beam splitter. Both signal beams were focused on an ICCD camera. The vertically polarized beam contained the plasma self-emission spectrum including the electron feature and its image is shown in Fig. 3(a). The horizontally polarized beam contained the plasma self-emission spectrum alone and its image is shown in Fig. 3(b). It must be noticed that the transmission efficiency of the spectrometer for the vertically polarized lights are about 2 times larger than that for the horizontally polarized lights. Therefore, the intensity spectrum for Fig. 3(b) was corrected by this factor and compared with that for Fig. 3(a) in Fig. 3(c). From Fig. 3(c), it can be seen that the intensity of the spectrum from Fig. 3(a) is slightly larger than that from Fig. 3(b) at around $\Delta\lambda$ =13 nm. Figure 3(d) shows a spectrum obtained by the subtraction of the two spectra. The T_e was decided from the peak wavelength of Fig. 3(d) and the n_e estimated by the ion feature as the first step. Since the scattered
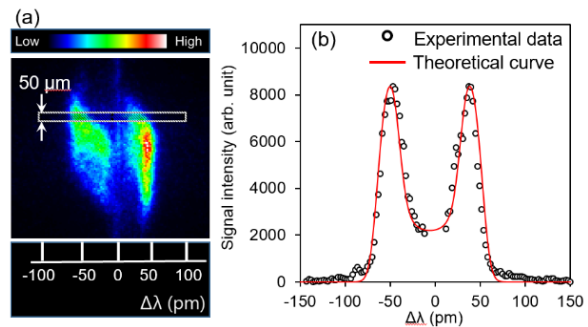

Fig. 2 (a) Ion feature image, (b) ion feature spectrum extracted from (a) and the theoretical curve fit
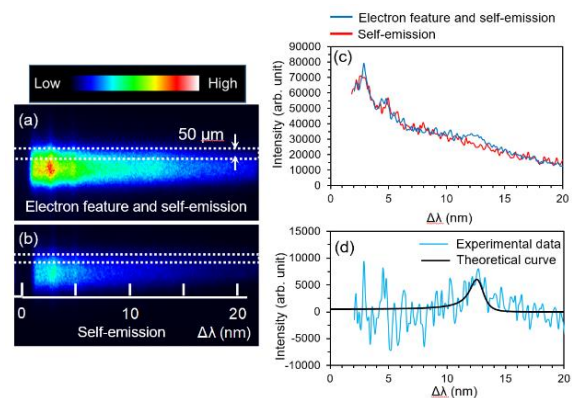

Fig. 3　Images of (a) the electron feature and the self-emission, and (b) the self-emission. (c) Spectra extracted from (a) and (b). (d) Spectrum of the electron feature.

light intensity of the ion feature weakly depends on T_e, several iterations were required to decide the values of n_e and T_e. Finally, n_e, T_e, T_i, and Z were decided to be 1.3×10^{24} m^{-3}, 33 eV, 25 eV, and 8.2, respectively.

5. Discussion

First, it was confirmed whether the electron feature intensity shown in Fig. 3(d) is consistent with the intensity of the ion feature. As described before, each intensity is proportional the dynamic form factors, therefore a ratio of the calibrated signal intensity must be equal to the ratio between S_i and S_e. Since the ion feature and the electron feature were detected by different detectors, absolute calibration was performed by Rayleigh scattering. As a result of the comparison, the signal intensity of the electron feature was about half of what was anticipated. We found that this is due to the vignetting reduction in the spectrometer and confirmed that the signal intensity at the $\Delta\lambda$ = 12 nm becomes about half of the signal at the center wavelength. Therefore, we conclude that the observed electron feature is plausible.

Second, the signal-to-noise ratio (SNR) of the electron feature is considered. When the present ICCD camera is used as the detector, a portion of the photons illuminating the photo-cathode is converted to photo-electrons (pe), which are accelerated toward the micro-channel-plate (MCP). These multiplied electrons impinge on a phosphor screen and they emit photons. These multiplied photons are converted to electrons by the charge-coupled-device (CCD). The electronic gain through the MCP is estimated to be as high as 10,000. Finally, a single photo-electron is output as 400 analog-to-digital units (ADU). Here, we calculate the number of photo-electrons detected under the measurements of the electron component of Thomson scattering. As shown in Fig. 3, the peak intensity of the electron component observed at around $\Delta\lambda$ = 12 nm was 6000 ADU. This signal intensity is equivalent to 15 pe. The dominant noise, in this case, is the shot noise which is due to the statistical fluctuation of single photo-electrons and is determined by the square root of the pe

number. As shown in Fig. 3(c), the total signal intensity of the plasma radiation at $\Delta\lambda$ = 12 nm is the order of 30,000 ADU. The shot noise based on both the Thomson scattering and the plasma radiation is calculated to be 11 pe. Therefore, the SNR is higher than one.

Third, we checked the value of T_e obtained by this experiment. The results show that T_e was 1.3 times higher than T_i. To discuss the validity of the difference, the electron heating by absorbing the probing laser (λ = 532 nm) is estimated. The method to evaluate the increment of T_e has been already discussed in previous papers[15-18], in which the processes of energy absorption by the inverse-bremsstrahlung and the heat diffusion to the volume surrounding the laser beam. Based on the calculations shown in Ref. 15, 16, it is found that an increase in T_e is at most 0.3 eV, which is less than 1% of the measured T_e. Then, we concluded that the effect of electron heating via the probing laser can be negligible.

Therefore, we finally concluded the signal observed here is really that of electron feature and gives a proper value of T_e to be 33 eV.

6. Conclusion

In this study, the ion feature and the electron feature of the laser-produced Sn plasma having parameters necessary for EUV light sources were detected simultaneously for the first time. The electron feature was observed with a SN ratio more than one, and found to be consistent with the ion feature giving a proper value of T_e.

References

1. U. Stamm, I. Ahmad, I. Balogh, H. Birner, D. Bolshukhin, J. Brudermann, S. Enke, F. Flohrer, K. Gäbel, S. Götze, G. Hergenhan, J. Kleinschmidt, D. Klöpfel, V. Korobotchko, J. Ringling, G. Schriever, C. D. Tran, and C. Ziener, Proc. SPIE **5037**, 119 (2003).
2. T. Higashiguchi, K. Kawasaki, W. Sasaki, and S. Kubodera, Appl. Phys.Lett. **88**, 161502 (2006).
3. K. Koshelev, V. Krivtsun, V. Ivanov, O. Yakushev, A. Chekmarev, V. Koloshnikov, E. Snegirev, and V. Medvedev, J. icro/Nanolithogr. MEMSMOEMS **11**, 021103 (2012).
4. H. Mizoguchi, H. Nakarai, T. Abe, K. M. Nowak,

Y. Kawasuji, H. Tanaka, Y. Watanabe, T. Hori, T. Kodama, Y. Shiraishi, T. Yanagida, G. Soumagne, T. Yamada, T. Yamazaki, S. Okazaki, and T. Saitou, Proc. SPIE 9422, 94220C (2015).

5. K. Nishihara, A. Sunahara, A. Sasaki, M. Nunami, H. Tanuma, S. Fujioka, Y. Shimada, K. Fujima, H. Furukawa, T. Kato, F. Koike, R. More, M. Murakami, T. Nishikawa, V. Zhakhovskii, K. Gamata, A. Takata, H. Ueda, H. Nishimura, Y. Izawa, N. Miyanaga, and K. Mima, Phys. Plasmas **15**, 056708 (2008).

6. A. Sasaki, A. Sunahara, H. Furukawa, K. Nishihara, S. Fujioka, T. Nishikawa, F. Koike, H. Ohashi, and H. Tanuma, J. Appl. Phys. **107**, 113303 (2010).

7. K. Tomita, Y. Sato, K. Nishikawa, K. Uchino, T. Yanagida, H. Tomuro, Y. Wada, M. Kunishima, T. Kodama, and H. Mizoguchi, Appl. Phys. Express **8**, 126101 (2015).

8. K. Tomita, K. Nakayama, K. Inoue, A. Sunahara, and K. Uchino, Appl. Phys. Express **6**, 076101 (2013).

9. Y. Sato, K. Tomita, S. Tsukiyama, T. Eguchi, K. Uchino, K. Kouge, H. Tomuro, T. Yanagida, Y. wada, M. Kunishima, T. Kodama, and H. Mizoguchi, Jan. J. Appl. Phys. **56**, 036201 (2017)

10. K. Tomita, Y. Sato, S. Tsukiyama, T. Eguchi, K. Uchino, K. Kouge, H. Tomuro, T. Yanagida, Y. wada, M. Kunishima, T. Kodama, H. Mizoguchi, A. Sunahara, and K. Nishihara, Sci. Rep. **7**, 12328 (2017)

11. T. Morita, Y. Sakawa, K. Tomita, T. Ide, Y. Kuramitsu, K. Nishio, K. Nakayama, K. Inoue, T. Moritaka, H. Ide, M. Kuwada, K. Tsubouchi, K. Uchino, and H. Takabe, Phys. Plasmas **20**, 092115 (2013).

12. E. R. Kieft, J. J. A. M. van der Mullen, G. M. W. Kroesen, V. Banine, and K. N. Koshelev, Phys. Rev. E **70**, 056413 (2004)

13. E. R. Kieft, J. J. A. M. van der Mullen, and V. Banine, Phys. Rev. E **72**, 026415 (2005).

14. D. H. Froula, S. H. Glenzer, N. C. Luhmann, Jr., and J. Sheffield, *Plasma Scattering of Electromagnetic Radiation* (Academic Press, New York, 2011) 2nd ed., Chap. 5.

15. K. Tomita, S. Hassaballa, and K. Uchino: Denki Gakkai Ronbunshi A 130 (2010) 1099 [in Japanese].

16. H. J. Kunze: Z. Naturforsch. A 20, 801 (1965).

17. Bentley R E, J. Phys. D: Appl. Phys. **30**, 2880 (1997).

18. Murphy A B, Phys. Rev. Lett. **89,** 025002 (2002).